journal of the mechanical behavior of biomedical materials 152 (2024) 106413

Contents lists available at ScienceDirect

Journal of the Mechanical Behavior of Biomedical Materials

journal homepage: www.elsevier.com/locate/jmbbm

Research paper

Improving early detection of keratoconus by Non Contact Tonometry. A computational study and new biomarkers proposal

Elena Redaelli [a,*], Michael Nana [c], Begoña Calvo [a,b], José Félix Rodríguez Matas [c], Giulia Luraghi [c], Jos Rozema [d,e], Jorge Grasa [a,b]

[a] Aragón Institute of Engineering Research (I3A), Universidad de Zaragoza, Zaragoza, Spain
[b] Centro de Investigación Biomecánica en Red en Bioingeniería, Biomateriales y Nanomedicina (CIBER-BBN), Zaragoza, Spain
[c] LaBS, Department of Chemistry, Materials and Chemical Engineering "Giulio Natta", Politecnico di Milano, Milan, Italy
[d] Visual Optics Lab Antwerp (VOLANTIS), Faculty of Medicine & Health Sciences, University of Antwerp, Antwerp, Belgium
[e] Department of Ophthalmology, Antwerp University Hospital, Edegem, Belgium

ARTICLE INFO

Keywords:
Keratoconus
Corneal biomechanics
Non Contact Tonometry
Fluid structure interaction simulations

ABSTRACT

Keratoconus is a progressive ocular disorder affecting the corneal tissue, leading to irregular astigmatism and decreased visual acuity. The architectural organization of corneal tissue is altered in keratoconus, however, data from *ex vivo* testing of biomechanical properties of keratoconic corneas are limited and it is unclear how their results relate to true mechanical properties *in vivo*. This study explores the mechanical properties of keratoconic corneas through numerical simulations of non-contact tonometry (NCT) reproducing the clinical test of the Corvis ST device. Three sensitivity analyses were conducted to assess the impact of corneal material properties, size, and location of the pathological area on NCT results. Additionally, novel asymmetry-based indices were proposed to better characterize corneal deformations and improve the diagnosis of keratoconus. Our results show that the weakening of corneal material properties leads to increased deformation amplitude and altered biomechanical response. Furthermore, asymmetry indices offer valuable information for locating the pathological tissue. These findings suggest that adjusting the Corvis ST operation, such as a camera rotation, could enhance keratoconus detection and provide insights into the relative position of the affected area. Future research could explore the application of these indices in detecting early-stage keratoconus and assessing the fellow eye's risk for developing the pathology.

1. Introduction

Keratoconus is an ocular disorder involving corneal tissue and it is classified as an ectatic corneal disease. Generally, the pathology has its onset at puberty and it develops until the third to fourth decade of life (Santodomingo-Rubido et al., 2022). It is characterized by progressive thinning and subsequent bulging of the outer structure, which can lead to irregular astigmatism of the corneal tissue in combination with decreased visual acuity. The altered external structure causes light to be scattered as enters the eye resulting in a low capability of focusing light and visual distortion. Treatment options for the disease vary depending on the stage of the condition. For mild cases, eyeglasses or contact lenses may be sufficient, however as the condition worsens, surgery such as a corneal transplant may be necessary to restore proper vision (Tan et al., 2012). The aetiology at the date is not fully understood (Blackburn et al., 2019). In literature, reviews evidence the dependency on both genetic and environmental factors (Romero-Jiménez et al., 2010), resulting in keratoconus being classified as a multifactorial disease. Meek et al. (1987) and Daxer and Fratzl-fx (1997) using X-ray scattering, identified two preferential directions for the collagen fibres in the healthy cornea, one orientation in the medial-lateral direction and another in the inferior–superior direction. Moreover, they noticed that as the collagen fibrils approach the limbus, they curve to run mainly around the periphery of the cornea. This regular orthogonal arrangement of the collagen fibrils is altered in keratoconic patients (Daxer and Fratzl-fx, 1997; Meek et al., 2005) and a gross rearrangement of vertical and horizontal collagen lamellae can be perceived. Analysis performed with confocal microscopy on excised pathological corneal buttons (Hollingsworth et al., 2005) highlighted the reduction in the density of the keratocytes in the stroma while second harmonic generated imaging proved the decrease of the number

* Corresponding author.
E-mail address: elena.redaelli@unizar.es (E. Redaelli).
URL: http://amb.unizar.es/people/elena-redaelli/ (E. Redaelli).

https://doi.org/10.1016/j.jmbbm.2024.106413
Received 16 October 2023; Received in revised form 8 January 2024; Accepted 17 January 2024
Available online 24 January 2024

of collagen lamellae (Morishige et al., 2007). The significant importance of keratocytes in maintaining the homeostasis of the cornea can explain the altered organization of the collagen lamellae while their reduction can be due to the increasing density of non-keratocytes that could be involved in the degradation of the collagen matrix (Ferrari and Rama, 2020). The orientation of the fibril layers is an important factor determining the mechanical properties of the cornea (Daxer and Fratzl-fx, 1997) and the loss in the orthogonally arranged pattern of collagen fibres is responsible for the weakening of the tissue (Meek and Boote, 2009). In pathological cases, the structure is less able to withstand the load and it becomes thinner under the intraocular pressure. For this reason, in progressive stages of keratoconus, the structure bulges leading to a non-uniform curvature of the outer-most surface. Despite this evidence in the architectural organization of keratoconic tissue, data from *ex vivo* testing of biomechanical properties of keratoconic corneas are limited and it is unclear how their results relate to true mechanical properties *in vivo*. Andreassen et al. (1980) showed that the mechanical strength of the cornea is reduced in keratoconus using uniaxial tensile tests. On the other hand, Nash et al. (1982) did not encounter a significant difference in the elastic behaviour of normal corneas with respect to keratoconus corneas for physiologically relevant stress levels. They instead highlighted that keratoconic corneas were weaker for high levels of strain. A number of studies (Blackburn et al., 2019; Ambekar et al., 2011; Vellara and Patel, 2015) reported that keratoconic corneas are weaker compared to normal corneas, however, none of them provide reliable information about their mechanical properties *in vivo*. Several techniques have been developed to investigate the mechanical behaviour of the corneal tissue *in vivo*. Non-contact tonometry (NCT) is an *in vivo* diagnostic procedure aimed at estimating the intraocular pressure (IOP) and the mechanical properties of the cornea. The load applied on the anterior surface of the eye by the air-puff, induces an inward deformation of the corneal structure followed by the recovery of its original shape in a bidirectional applanation process, passing through three times of interest: the first applanation (A1), the highest concavity (HC) and the second applanation time (A2) (Lopes et al., 2021). Corvis ST® (OCULUS, Wetzlar, Germany) (Guide, 2020) is a commercially available tonometer that employs an ultra-high-speed camera to capture images of the section of the cornea in the nasal-temporal (NT) plane during the 30 ms duration of the air puff, with a frequency of 4330 frames per second (De Stefano and Dupps, 2017). The downward displacement of the structure is tracked, and a number of clinical biomarkers are derived and output for the analysis. To detect the presence of keratoconus from the results of Corvis ST, different indexes have been proposed. Vinciguerra et al. (2016, 2017) introduced the Corvis Biomechanical Index (CBI) based on various dynamic corneal response parameters obtained from Corvis ST. The index can successfully differentiate between keratoconic and healthy eyes in 98% of the analysed cases (Vinciguerra et al., 2016). In 2017, Roberts et al. (2017) proposed an index to evaluate the stiffness of the corneal tissue, the stiffness parameter A1 (SP-A1). The SP-A1 is the difference between the adjusted air pressure over the cornea at first applanation time and the biomechanically corrected IOP (bIOP (Eliasy et al., 2023)), divided by the deflection amplitude at first applanation time. Zhao et al. (2019) observed a decrease in SP-A1 in keratoconic patients. Both the CBI and the SP-A1 are only useful to classify healthy from keratoconic patients without giving any information about the mechanical properties of the pathological tissue and they are based only on the analysis of the NT section of the cornea. Furthermore, the deformation of the eye in response to the applied air puff in Corvis ST depends on four main factors: the IOP, the load applied on its outer surface, the thickness of the cornea and the mechanical properties of the eye ball and surrounding tissues (Ariza-Gracia et al., 2016). The need of computational simulations is related to the possibility of uncoupling the four contributions and to analyse the influence of each component on the data obtained in clinical practice. Moreover, with a 3D model it is possible to analyse the entire behaviour of the corneal structure, and not only its NT section, highlighting its anisotropic behaviour.

This paper aims to evaluate the effectiveness of the current clinical biomarkers used in Corvis-ST in detecting early-stage keratoconus and establishing a relationship between these biomarkers and the mechanical properties of the pathological corneal tissue. In the initial stage of keratoconus, the ongoing alterations in the internal structure of the tissue are not reflected in its outer appearance, making it challenging to identify the presence of the pathology only by means of topographic analysis. Besides the computation of the biomarkers currently in use, a double-sectional analysis coupled with an asymmetry-based approach is proposed. A Fluid-Structure Interaction (FSI) simulation is implemented in ANSYS Ls-Dyna (Dev, 2023) following the methodology outlined in our previous work (Redaelli et al., 2022). The work is systematically planned into three main sensitivity analyses to investigate the single influence of three key elements of the model: corneal material properties, size, and location of the keratoconic area. The outputs of each simulation are then compared with the results of the healthy geometry, used as a benchmark to evaluate the effect of the pathological mechanical properties. A clinical analysis is also performed to evaluate the effectiveness of the proposed indexes in a real scenario.

2. Materials and methods

2.1. Numerical model of the NCT

The NCT is modelled using an FSI simulation implemented in the finite-element solver LS-Dyna R14.0 (ANSYS, Inc., Canonsburg, PA,United States) (Dev, 2023). All the simulations described are performed using an Intel i9-10940X (3.30 GHz) on 14 CPUs, the average computational time of each simulation is 48 h. The whole model comprises both a solid and a fluid part, to couple the downward displacement of the eye with the pressure applied by the incoming air jet. Fig. 1.a illustrates the 3D structure of the eye used in the simulations; the geometry comprises cornea, limbus, sclera, and humours. The crystalline lens, the ciliary zonule and the vitreous membrane are not included in the model since we demonstrated in our previous work (Redaelli et al., 2022) that they do not have an important influence on the corneal deformation during the NCT. The components are discretized with fully integrated hexahedral solid elements. The humours are represented as a cavity simulating an incompressible fluid, with an initial IOP set at 15 mmHg. Throughout the simulation, the IOP is subject to variation: the incompressibility condition dictates that the volume of the humours remains constant; consequently, the corneal deformation induced by the air puff is sustained by an increase in IOP. The cornea and the limbus are described as anisotropic, nearly incompressible, hyperelastic materials, to account for the influence given by the network of collagen fibres. The cornea is described with two families of mutually orthogonal collagen fibres assumed perfectly aligned with the nasal-temporal (NT) and superior-inferior (SI) direction and the limbus is described with one circumferential family of fibres as shown in Fig. 1.b. In both cases, the Holzapfel–Gasser–Ogden (Holzapfel et al., 2000) constitutive model is used. Eq. (1) shows the isochoric contribution of this model to the free energy.

$$\bar{\Psi} = C_{10}(\bar{I}_1 - 3) + \frac{k_1}{2k_2}\sum_{i=4,6} e^{k_2(\bar{I}_i - 1)^2} \tag{1}$$

where C_{10}[MPa] is a material parameter related to the extracellular matrix behaviour, k_1[MPa] refers to the stiffness of the fibres and k_2[-] models their non-linearity. I_1 is the first invariant of the right isochoric Cauchy–Green stress tensor, while I_4 and I_6 are respectively the fourth and the sixth pseudo-invariants related to the fibres stretch. The sclera is modelled as a nearly incompressible hyperelastic isotropic material with a Neo-Hookean formulation. The material parameters of the healthy eye tissues incorporated in the finite element model are listed in Table 1.

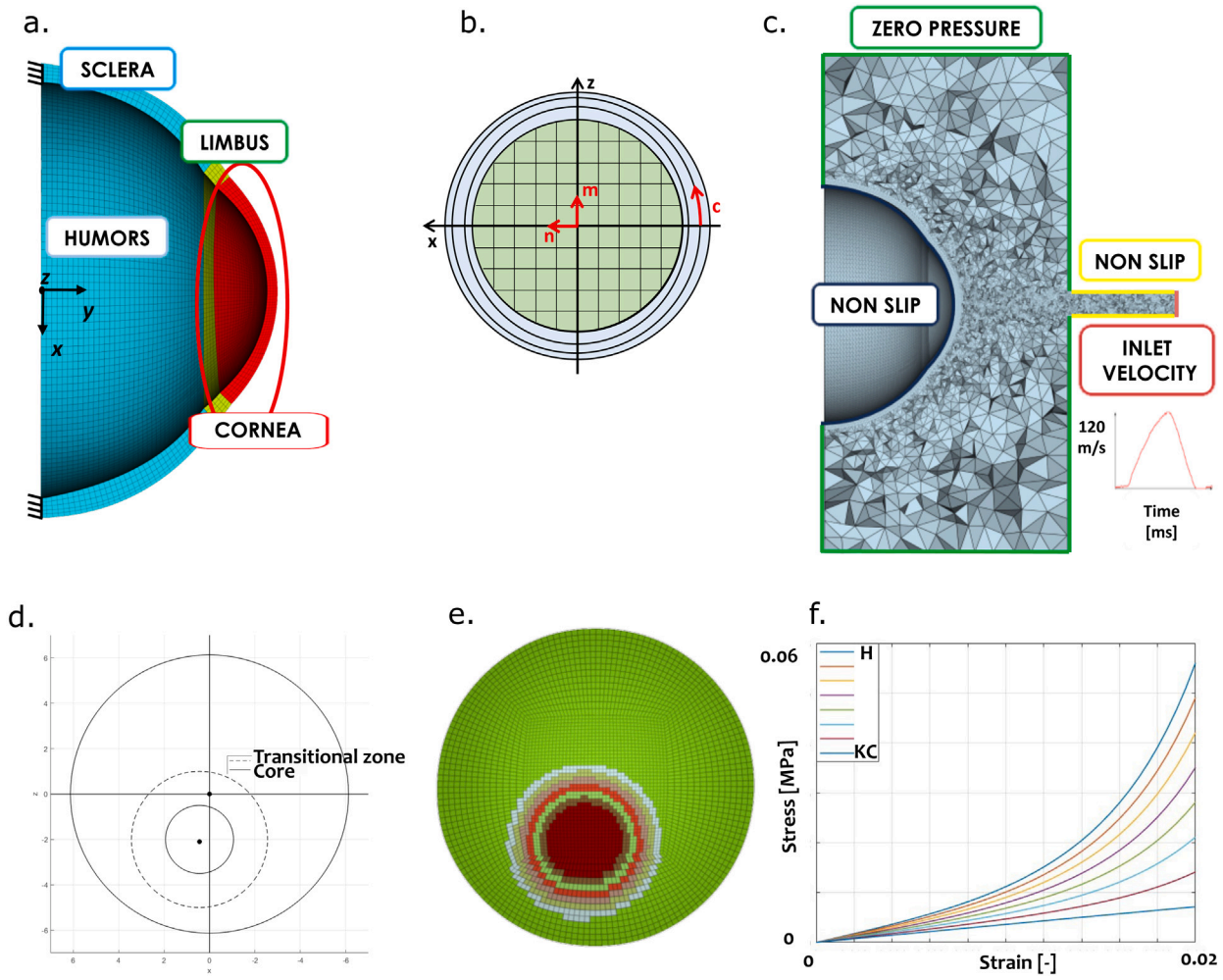

Fig. 1. Numerical model of the Non Contact Tonometry: (a) structural model and boundary conditions; (b) assumption on collagen fibres distribution on cornea and limbus; (c) Fluid model and boundary conditions; (d) Pathological corneal model where the transitional region and the core of the pathological region are highlighted in the Inferior-Nasal quadrant; (e) Mesh of the pathological corneal model, the transitional zone is composed of six rings of elements. (f) Stress strain response of the pathological (KC), transitional and healthy(H) zones. In the model, a left eye is considered.

Table 1
Material parameters of the healthy eye tissues incorporated in the finite element model.

	C_{10} [MPa]	k_1 [MPa]	k_2 [-]	Ref
Cornea	$1.80 \cdot 10^{-2}$	$1.26 \cdot 10^{-1}$	$9.34 \cdot 10^{2}$	Redaelli et al. (2022)
Limbus	$2.50 \cdot 10^{-2}$	$1.00 \cdot 10^{-2}$	$1.00 \cdot 10^{2}$	Redaelli et al. (2022)
Sclera	$8.00 \cdot 10^{-1}$	–	–	Redaelli et al. (2022)

As the eye geometry pertains to the pressurized configuration, each simulation employs an iterative algorithm (Ariza-Gracia et al., 2016) to establish the stress-free configuration, which is then subjected to the IOP.

On the other hand, the air is simulated as an incompressible fluid with a density of $\rho = 1.25$ kg/m^3 and a dynamic viscosity of $\mu = 1.8 \cdot 10^{-5}$ Pa· s. The mesh and boundary conditions for the fluid domain are depicted in Fig. 1.c. First, a simulation is run with the healthy values of the corneal tissue. This simulation modelled the physiological scenario is denominated as PHY. Then, simulations corresponding to the pathological cornea are performed.

With reference to Pandolfi and Manganiello (2006), keratoconus is designed as a rounded diseased tissue with a core of 1.5 mm in radius and a transitional area of 1.5 mm in width that is divided into six circular zones as shown in Figs. 1.d and 1.e. Hence, the total pathological tissue has a diameter of 3 mm. This size is used for all analysis except for the sensitivity analysis where this dimension is varied. Keratoconus typically arises in the Inferior-Nasal region of the eye during its initial stages (Eliasy et al., 2020), therefore, the pathological area is modelled in the Inferior-Nasal region, corresponding to the negative x-axis ($x = -0.4$ mm) and positive z-axis ($z = 2$ mm) as shown in Fig. 1.d. In the numerical simulation, a left eye is considered. The central region of the rounded diseased tissue is modelled as an isotropic, nearly incompressible hyperelastic material using a Neo-Hookean formulation with the same C_{10} reported for the corneal tissue in Table 1. This approach aims to replicate the loss of the architectural organization of the collagen fibres (Meek and Boote, 2009). The six transitional zones are intended to provide a smooth progression from the healthy anisotropic tissue of the cornea to the completely isotropic tissue of the centre of the disease. With this intention, the parameter related to the stiffness of the collagen fibres k_1 is decreased linearly from 0.1265 [MPa] (healthy) to zero (pathological). The stress strain response of the zones considered is shown in Fig. 1.f.

2.2. Sensitivity analyses

2.2.1. Material sensitivity analysis

The first sensitivity analysis aims to evaluate the influence of the mechanical properties of the pathological area on the NCT results. For this purpose, the size and the location of keratoconus are kept constant, in particular, the centre is in $x = -0.4$ mm and $z = 2$ mm and the radius of the entire pathological area is 3 mm. Three different mechanical

Table 2
Stiffness of the extracellular matrix in the pathological area of the three models of the material sensitivity analysis. TEM: template material model, INC: increased material model, DEC: decreased material model.

Pathological model	C_{10} [MPa]
TEM	$1.80 \cdot 10^{-2}$
INC	$2.40 \cdot 10^{-2}$
DEC	$1.20 \cdot 10^{-2}$

properties of the same material model are designed for this analysis. In the three pathological models, the mechanical behaviour of the core of the disease is kept hyperelastic isotropic but different values of C_{10} are applied, to model different degrees of severity conditions. In the Template material model (TEM), C_{10} describing the response of the pathological area is of the same value as for the healthy tissue, while in the Increased material model (INC) and Decreased material model (DEC) the parameter is respectively increased or decreased by one third to describe a damaged tissue. The values of C_{10} used in the material sensitivity analysis are reported in Table 2.

2.2.2. Size sensitivity analysis

The purpose of the size sensitivity analysis is to simulate the progression of the pathology. To achieve this, the size of the keratoconus (comprising both the core and the transitional area) is reduced to radii of 2 mm and 1.5 mm, as illustrated in Fig. 2.a. Consistent with the previous analyses, the centre of the rounded diseased tissue is kept in $x = -0.4$ mm and $z = 2$ mm, and the material parameters of the TEM model are assigned to each geometry to evaluate the influence of only size and assess the presence of a threshold value below which the pathology cannot be detected by the device.

2.2.3. Location sensitivity analysis

The last analysis performed is intended to examine the effect of the location of the pathological area. The TEM is renamed *"centred model"* and the output data obtained are compared with the *"shifted model"* obtained by displacing the initial pathological area on the bisector of the Nasal-Inferior quadrant of the left eye and keeping the same distance to the apex of the cornea (see Fig. 2.b). The positions of the centred and shifted models depicted in Fig. 2.b, corresponds to $x = -0.4$ mm for the initial position and $z = -1.75$ mm and to $x = -1.75$ mm and $z = 2$ mm for the shifted centre position.

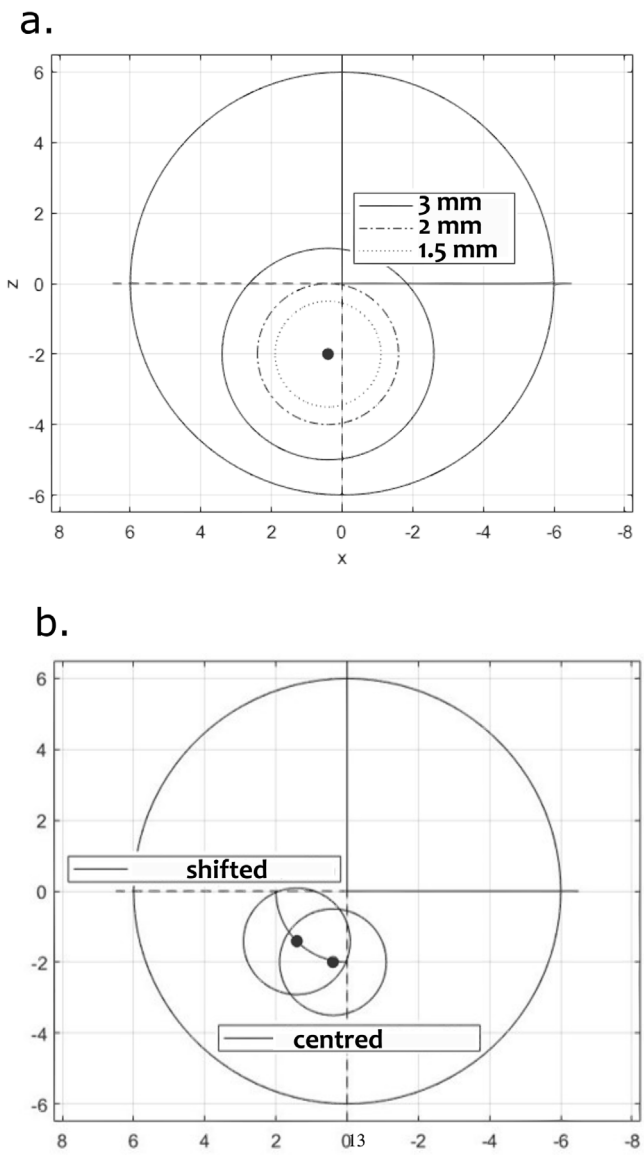

Fig. 2. (a) Dimension of the pathological areas in the size sensitivity analyses; (b) Position of the pathological areas in the location sensitivity analyses. Keratoconus centre is placed in the Nasal-Inferior quadrant.

2.3. Biomarkers

The computational approach provides the possibility to track and register the time evolution of all the nodes of the corneal model. However, to make the simulation results comparable with the clinical results, three Corvis-ST biomarkers are selected and evaluated in the NT plane of each computational model:

- Deflection amplitude, which is the downward displacement of the corneal apex with respect to its initial position (Fig. 3.a).
- Delta arc length, which represents the difference between the length of a meridional section of the anterior surface computed between −3.6mm and 3.6 mm in the initial configuration and the same length at HC (Fig. 3.b).
- Peak distance, which is the horizontal distance computed between the right and left peaks in the HC configuration (Fig. 3.c).

Among these biomarkers, only the deflection amplitude is tracked over time, and its peak value is used to determine the HC moment during the simulation.

In addition to the NT section captured by the device, from the simulations the SI section is also analysed and the respective biomarkers are computed. The nodes of the NT section coincide with the nodes of the anterior surface of the cornea that belongs to the xy plane of the system, whereas for the SI section corresponds the yz plane (Fig. 1.d). The two configurations are analysed in time during the air jet every 0.2 ms, which coincides with the frequency of the Corvis ST camera. Besides the abovementioned clinical biomarkers, at the HC instant, vertical and horizontal asymmetry indexes are defined with the purpose of better characterizing the influence of the diseased tissue on the corneal response. From an initial in silico analysis of the pathological cornea during the NCT, an evident asymmetry in the deformation has been seen and the need to have indexes to quantify this asymmetry became evident. Along both sections, the horizontal position of the lowest point of the anterior surface is captured and stored in the Sym_h index (Fig. 3.d), while the difference in height between the positive and negative peaks of the configuration is defined as Sym_v (Fig. 3.e). The results of both the biomarkers and the asymmetry indexes are always compared with the pixel dimension of Corvis ST images (14 μm) to assess if the difference evaluated in the simulation can be observed by analysing the clinical images.

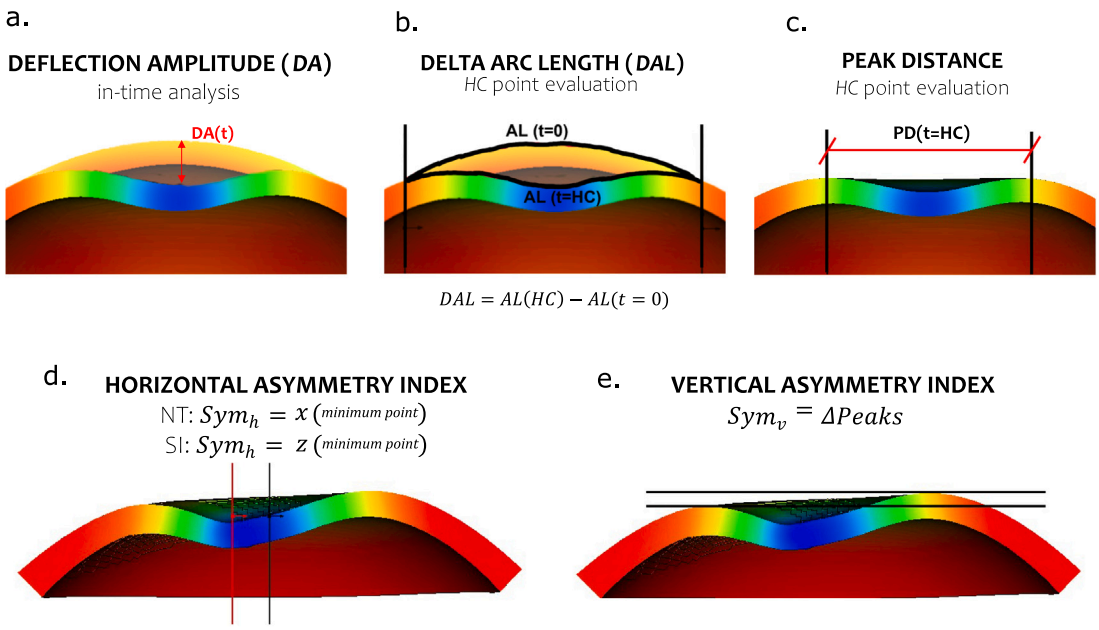

Fig. 3. Graphical representation of the biomarkers analysed in both the NT and the SI sections: (a) Deflection amplitude, (b) Delta Arc Length, (c) Peak Distance, (d) Horizontal asymmetry index, (e) Vertical asymmetry index.

2.4. Clinical analysis

Six clinical cases with pathological corneas are analysed using both the topographic maps of Pentacam (OCULUS, Wetzlar, Germany) (Hr, 2020) and their Corvis ST results. The data used were randomly selected from a previous study conducted at Antwerp University Hospital (reference number of the Antwerp University Hospital Ethical Committee: 17/12/136). That study was conducted following the principles of the Declaration of Helsinki, and participants provided signed informed consent before measurement. The analysed patients present late-stage keratoconic corneas with visible changes in axial curvature within the pathological zone. Two left eyes and four right eyes are considered. In the FEM model, a left eye has been considered. For all patients, the initial corneal profile and the profile at the time of HC are detected to determine if any asymmetries can be observed. The Sym_h and the Sym_v indexes are calculated for each patient at HC, and the relationship between the position of the pathological area and the asymmetry indexes is assessed.

3. Results

3.1. Material sensitivity analysis

The displacement fields captured at the HC time on the anterior surface of the cornea are depicted in Fig. 4.a for all the designed pathological models, alongside the data obtained for the healthy geometry. A trend of increasing values of downward displacement is evident, and it is consistent with the material weakening. This trend can also be appreciated by analysing the computed values of three biomarkers in Fig. 4.b. The deflection amplitude increases with the weakening of the pathological tissue. The values of the computed peak distance and delta arc length exhibit significant alterations compared to the healthy data, with a remarkable increase in magnitude in the SI section of the analysis. In particular, with the weakening of the tissue, the peak distance increases, and the delta arc length decreases. The anterior surface profiles at HC depicted in Fig. 4.c underline a non-symmetrical downward displacement induced by the degeneration of the tissue. The values of Sym_h reported in Table 3 show how the lowest point of each pathological configuration is shifted towards the positive values of x along the NT section and the negative values of z along the SI section, consistent with the position of the centre of the pathological tissue. This leads us to the conclusion that the weaker the mechanical properties of the tissue, the closer the minimum point is to the centre of the pathological area. The analysis of the Sym_v index in Table 3 indicates that all the models exhibit a difference in height between the peaks of the HC configuration, with the lowest peak captured in the positive values of x along NT and on the negative value of z along SI. To assess the detectability of the variations computed by the indexes, their magnitude should be compared with the resolution of the clinical images characterized by squared pixels of 14 μm. Since the values of all the indexes are higher than 14 μm, they can also be potentially used in a clinical analysis. We have introduced a progressive colour scale ranging from green to red to map the Sym_v index, enabling a rapid visual assessment of the severity of the asymmetry. The scale is depicted in Fig. 5 and it is defined based on the conversion of the index to pixels. This scale is not applied to the Sym_h index because the value of this index is related to the position of the pathological area, not to its gravity.

Table 3
Asymmetry indexes of the models evaluated in the material sensitivity analysis. The values of Sym_h of the NT section are positive, while the values of Sym_h of the SI section are negative consistent with the position of the centre of the pathological tissue. The values of Sym_v are filled with colours defined in the severity scale of Fig. 5.

		INC	TEM	DEC
Sym_h [mm]	NT	0.1321	0.1436	0.1513
	SI	−0.6305	−0.6624	−0.9141
Sym_v [mm]	NT	0.0639	0.0711	0.0787
	SI	0.1815	0.1007	0.1742

3.2. Size sensitivity analysis

The progressive reduction of the size of the keratoconus (diameter reduced from 3 to 1.5 mm) results in a progressive reduction of corneal deformation as shown in Fig. 6.a (The healthy case and the pathological case with a radius of 1.5 mm are highlighted). From the analysis of

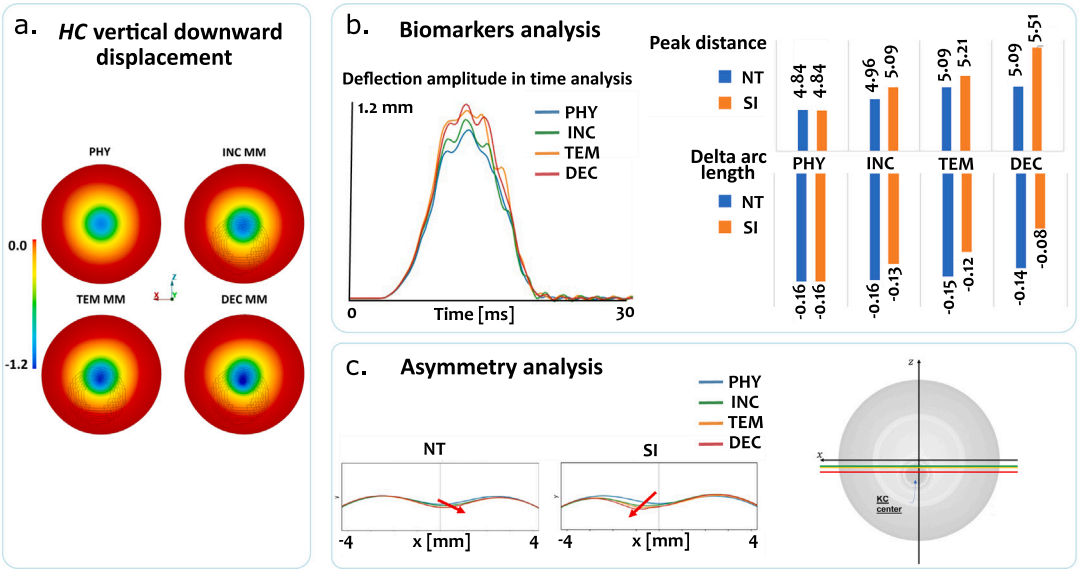

Fig. 4. Material sensitivity analysis: (a) Contour of vertical displacement [mm] captured at HC time on the anterior surface of the cornea in the healthy case (PHY), in the template material model (TEM), in the increased material model (INC) and the decreased material model (DEC); (b) Corvis ST biomarkers evaluated in the four models; (c) Asymmetry analysis at highest concavity.

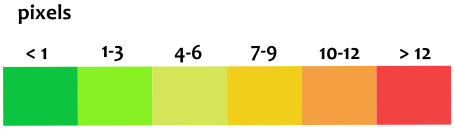

Fig. 5. Scale colour introduced to visualize in the Symv index the severity of the pathological area.

the deflection amplitude of the apex of the cornea during the test depicted in Fig. 6.b, evince how halving the size of the damaged area to 1.5 mm leads to a deflection amplitude similar to the healthy case, with differences between the peaks of the curves of less than 2% mostly associated with numerical oscillation due to the numerical simulation. This is strengthened by the almost identical values of the peak distance, with a maximum difference of 0.3% on the SI direction, and the complete symmetrical downward displacement depicted in the asymmetry analysis of Fig. 6.c. The alterations due to the size of the keratoconus are of the order of one pixel, resulting undetectable by the segmentation technique used to analyse clinical images. When instead the radius of the pathological area is 2 mm, there are detectable differences both in the biomarkers and in the asymmetry indexes. This result highlights that there is a minimum size below which the NCT is not able to detect the presence of the pathology even using other sections of analysis and the new biomarkers.

3.3. Location sensitivity analysis

The displacement of the anterior surface of the cornea at HC (Fig. 7.a) and the biomarkers calculated in the NT section (Fig. 7.b) do not show important differences between the two models. More relevant variations can be appreciated by comparing the biomarkers in the SI section. Moreover, the Sym_h values of the two geometrical models are different. The shifted model registers the lowest point of the HC configuration in $x = -0.375$ mm and $z = 0.551$ mm, showing a remarkable asymmetrical downward displacement along both sections of the analysis. The SI and NT sections at HC configurations are depicted in Fig. 7.c along with vertical lines passing through the lowest points. The centred model exhibits a lower asymmetrical displacement along NT, where the lowest point is in $x = 0.14$ mm, while a higher asymmetrical degree on the perpendicular section can be seen by the Sym_h index equal to -0.663 mm.

3.4. Clinical analysis

The Pentacam axial maps of the patients analysed are shown in Fig. 8.a. The prevalence of the pathology in the Nasal-Inferior quadrant of the eye can be highlighted, demonstrating that our model represents the correct location of the disease. Fig. 8.b shows that the highest deformation amplitude is reported for patients 53 and 92 who also have a steepest pathological area visible in the Pentacam maps. In those two patients, the pathological area covers almost the entire inferior part of the cornea, with an equivalent radius reaching 4 mm, higher than the one used in the simulations. The deformation amplitude is a Corvis ST biomarker defined as deflection amplitude plus whole-eye movement. Our material sensitivity analysis has shown that the deflection amplitude is higher for the weaker pathological tissues. This clinical evidence highlights that the more protruded the cornea, the weaker the underlying pathological tissue. Regarding the asymmetry of the structure, Fig. 8.a shows the corneal profiles at the initial configuration and at HC. Even if all the eyes are initially with a symmetric and centred shape, at HC they present an asymmetry both horizontally and vertically. The green line highlighting the Sym_h index shows that horizontally the asymmetry is not very evident because the position of the centre of keratoconus in the eyes considered is located near the vertical axis. In these cases, an analysis of the SI section of the cornea, as in our numerical analysis, could be useful to differentiate the patients. The Sym_h indexes reported in Table 4 present both positive and negative values depending on the position of the centre of keratoconus but they are close to zero. The Sym_v indexes reported in Table 4, show an increasing value with the increase of the area affected by the pathology. In particular, patient 110, which presents the largest pathological area has the highest value of Sym_v. In treating clinical data it is worth noting that right and left eyes are detected in different orientations by Pentacam and Corvis. The Nasal-Inferior region for right eyes (as patients 19, 53, 103, 110) is the fourth quadrant of the screen, while for left eyes Nasal-Inferior region is in the third quadrant of the screen.

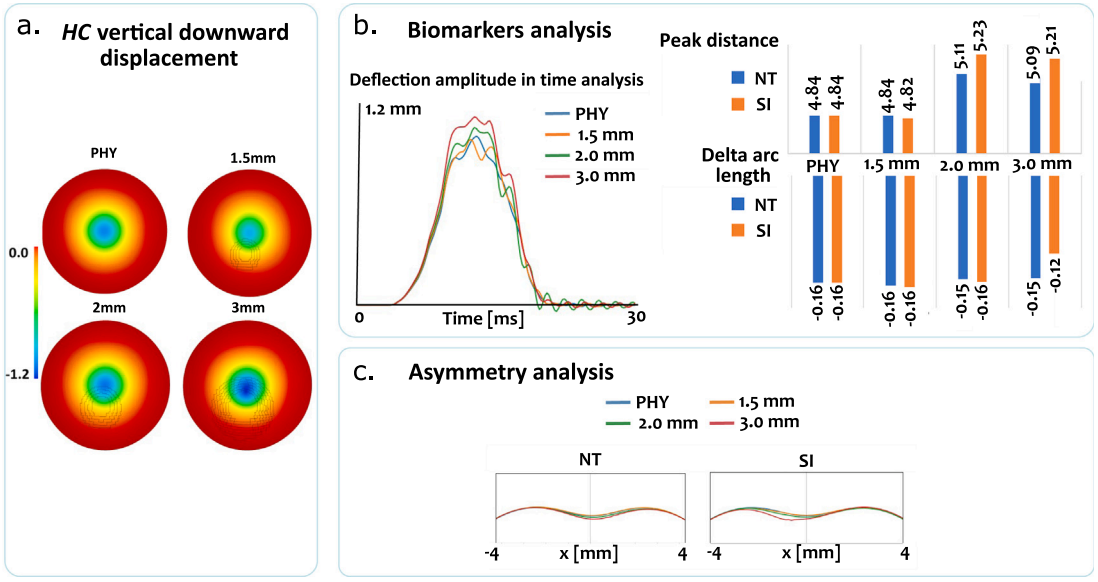

Fig. 6. Size sensitivity analysis. (a) Contour of vertical displacement [mm] captured at HC time on the anterior surface of the cornea in the healthy case (PHY), and with different radii of the pathological area; (b) Corvis ST biomarkers evaluated in the four models; (c) Asymmetry analysis at highest concavity. The results are highlighted for the healthy case and the pathological case of 1.5 mm diameter to show that there is no difference between them.

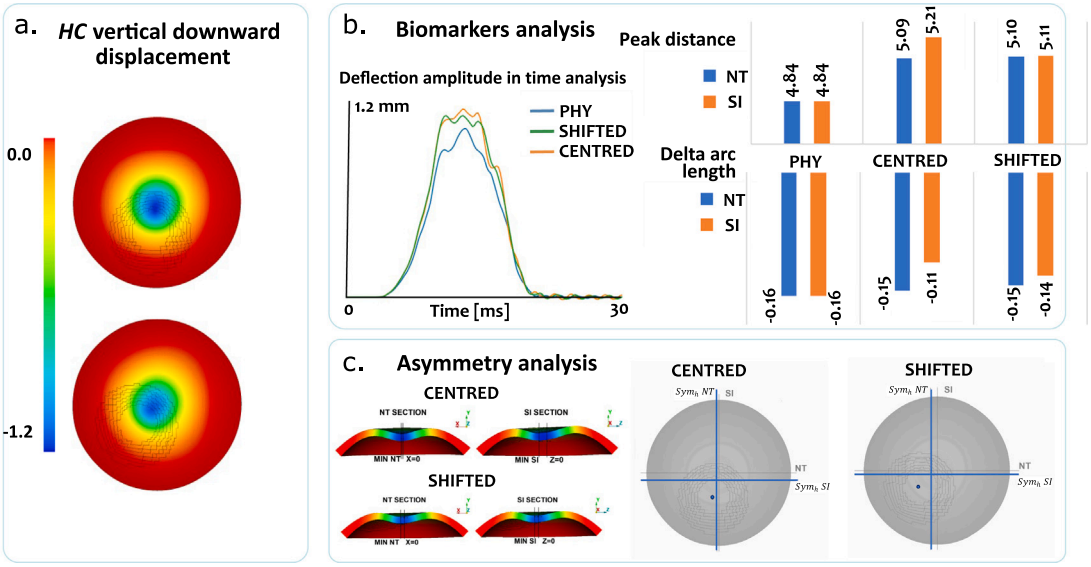

Fig. 7. Location sensitivity analysis. (a) Contour of vertical displacement[mm] captured at HC time on the anterior surface of the cornea in the centred and shifted models; (b) Corvis ST biomarkers evaluated in the four models; (c) Asymmetry analysis at highest concavity.

Table 4
Horizontal and vertical asymmetry indexes for the patients analysed. The values of Sym_v are filled with colours defined in the severity scale of Fig. 5.

Patient number	Sym_h [mm]	Sym_v [mm]
19	0.130	0.162
53	−0.234	0.101
66	−0.136	0.101
92	0.102	0.062
103	−0.248	0.108
110	−0.290	0.173

4. Discussion

The increasing incidence of keratoconus and its clinical implications have sparked interest in modelling and characterizing the mechanical properties of pathological corneas through new devices and numerical simulations which are useful for describing the corneal dynamic response. In their work, Anderson et al. (2004) developed a finite element model of a keratoconic cornea, wherein the pathological area was characterized by a gradual loss of thickness. They modelled the corneal behaviour during Goldamann Applanation Tonometry (GAT), founding an increased corneal deformation as a result of the disease and they highlighted that the distribution of the deformation is dependent on the location of the pathological area. Our analysis has shown that the behaviour of the keratoconic cornea during Corvis ST is in line with its behaviour during GAT. However, their modelling of the diseased tissue focused solely on reducing the thickness of the structure without

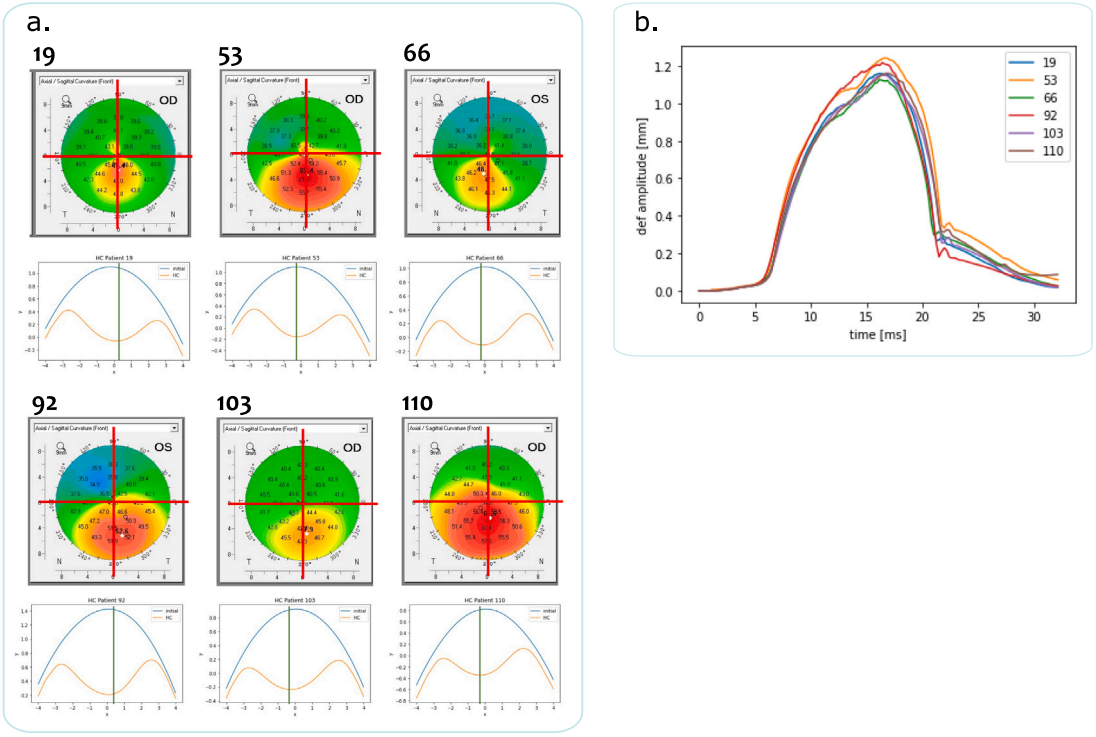

Fig. 8. (a) Pentacam maps showing the axial curvature of the anterior corneal surface of each patient. The initial and HC configuration of the same corneas during Corvis ST are shown below each map. The green line shows the position of the minimum point. (b) deflection amplitude in time for each patient evaluated by the Corvis ST device.

studying the influence of the material properties. Gefen et al. (2009) examined the mechanical behaviour of the keratoconic cornea using a simulated inflation test, modifying the parameters of the healthy orthotropic material model alongside a thickness reduction to represent the pathological tissue. They underlined that the combination of tissue thinning, and degraded material properties is involved in the pathogenesis of keratoconus, leading subsequent works to concentrate the analysis on the pathological mechanical properties. Pandolfi and Manganiello (2006) employed the Holzapfel–Gasser–Ogden equation to model the corneal tissue as a fibre-matrix reinforced material. They proposed to lower the parameters of the healthy model when simulating the keratoconus and they compared the results of their simulations with experimental uniaxial tensile tests and inflations tests, demonstrating that the lowering of the mechanical properties of a region of the cornea could describe in a reliable way the behaviour of keratoconic corneas. For this reason, the same approach has been adopted in this paper, together with the approach adopted in Roy and Dupps (2011) in which, to simulate the response of keratoconic corneas to collagen cross-linking patterns, the centre of the pathological area was considered isotropic. In a more recent publication, Giraudet et al. (2022) investigated the origin of keratoconus pathology comparing in a simulation the change in pathological geometry and mechanical properties. They tested the influence of small variations of each mechanical parameter of an anisotropic material model on the corneal deformation during an inflation test, and they observed that the most sensitive parameter is the unfolding stretch, that is the stretch at which the fibrils start to generate force. This result supports our choice of isotropic behaviour of the core of the pathological cornea.

To the best of our knowledge, this is the first study dealing with the numerical simulation of NCT on a keratoconic eye. During the NCT, the cornea undergoes non-physiological deformation, enabling the evaluation of its response at high levels of strain. Since the first stage of keratoconus is characterized by alterations in the fibres organization, which impact the corneal response at high levels of strain, establishing a connection between the mechanical properties of the corneal tissue and the results of the NCT test could be of great interest for early-stage pathology detection (Santodomingo-Rubido et al., 2022). We have presented three sensitivity analyses regarding the influence of mechanical properties, size and location of the pathological area on the outputs of a commercially available NCT, the Corvis ST. Our analysis goes beyond the typical focus on the NT section of the cornea of Corvis ST. We have proposed a double sectional analysis, which allows for a deeper examination of corneal deformations. This approach is supported by previous research by Curatolo et al. (2020) and Li et al. (2023), which showed that exploring multiple meridians reveals important differences between keratoconic and normal eyes. In particular, Curatolo et al. (2020) proposed a customized OCT system coupled with a collinear air-puff excitation unit, capable of acquiring dynamic corneal deformation on multiple meridians, both in *ex vivo* and *in vivo* eyes demonstrating that the early-keratoconic eyes show a higher apical displacement, as well as a distinct asymmetry between the vertical and horizontal meridians. On the other hand, Li et al. (2023) explored different meridians showing that the differences between the keratoconic and normal eyes in the SI and SN-IT meridians were increased compared to the NT meridian.

Our study extends the idea of these papers by introducing two new indices, the horizontal asymmetry index (Sym_h) and the vertical asymmetry index (Sym_v), which further enrich our understanding of corneal asymmetry in pathological conditions. In the material sensitivity analysis, the fields of downward displacement captured at HC, reflect the increasing compliance induced by the presence of the keratoconus. The magnitudes of the computed biomarkers are significantly altered when compared with the benchmark results obtained from the healthy geometry on both sections of analysis. These parameters exhibit a persistent increment in SI, resulting from the fixed position of the damaged tissue that crosses the SI section. This higher influence is confirmed by the asymmetry-based analysis. The Sym_h value shows an increase in amplitude with the weakening of the tissue towards the coordinate of the core of the rounded diseased tissue, centred in $z = -2$ mm. In the size sensitivity analysis, we found that Corvis ST in

Table 5
Correspondence between the values of the horizontal asymmetry indexes and the centre of the pathological area.

Eye	Sym_h in the NT section	Sym_v in the SI section	Keratoconus centre position
Left	–	+	NASAL-INFERIOR
Left	–	–	NASAL-SUPERIOR
Left	+	+	TEMPORAL-INFERIOR
Left	+	–	TEMPORAL-SUPERIOR
Right	–	+	TEMPORAL-INFERIOR
Right	–	–	TEMPORAL-SUPERIOR
Right	+	+	NASAL-INFERIOR
Right	+	–	NASAL-SUPERIOR

unable to detect pathological areas with a diameter lower than 1.5 mm. The unaltered deformation behaviour of the 1.5 mm model with respect to the healthy behaviour, is given by the combination of two separate factors. The acquired data resulted from both the halving of the initial size of the diseased tissue and the increased distance of the tissue from the area subjected to the applied pressure load. This increased distance is due to the fixed position of the centre of the rounded diseased tissue. The last analysis evaluates the accuracy of the proposed asymmetry indexes to locate the pathological tissue. In both geometries tested, the clinical biomarkers were significantly apart from the healthy ones, emphasizing how these variations could lead to the detection of the pathology but without providing suitable details regarding the location of the affected area. Instead, the data obtained from the asymmetry-based analysis can be integrated for deriving position information on the direction of maximum displacement of the anterior surface of the cornea. In each model, combining the values of the Sym_h parameter computed along the two sections of analysis a point on the outer surface of the tissue can be derived and assumed as a guide to identifying the affected region. The values computed in both models are in fact directed towards the centre of the designed rounded diseased tissue.

Given that our findings are based on a numerical simulation of a left eye, the results from such analyses should be treated with caution. In a left eye, according to our reference system, the Nasal-Inferior quadrant corresponds to the negative values of the x-axis and positive values of z-axis. In a right eye, instead, the Nasal-Inferior quadrant correspond to positive x-axis and positive z-axis. While the Sym_v index is always positive, we demonstrated that the sign of the Sym_h index gives information about the position of the centre of the pathological area. To avoid misunderstandings about the position, Table 5 relates the sign of the horizontal asymmetry index with the position of the pathological area.

We aware that out research may have some limitations. The absence of available in-vivo data on the mechanical properties of corneal tissue compelled us to assume a completely isotropic behaviour when modelling the core of keratoconus. This assumption is supported by the evidence that the arrangement of the collagen fibres is lost in pathological conditions. Nonetheless, more reliable experimental data about the mechanical stress–strain response of the keratoconic tissue could significantly enhance our ability to compare the mechanical model's performance against the real scenario. In this study, only the early stage of keratoconus has been considered, no geometrical changes of the cornea have been incorporated in the pathological model. A future step could be the study of the influence of the geometrical changes on the output of the NCT simulation. Furthermore, uniform corneal material behaviour throughout the thickness was assumed. The sensitivity analysis conducted did not account for material properties variability, which may play a role in corneal deformation. Future studies could delve into the implications of material property variations across the thickness and mid-surface of the cornea. Notably, given that keratoconus initiates in the posterior corneal surface before extending to the anterior surface, investigating the influence of keratoconus progression could be a promising direction for further exploration in this study. However, this step would introduce more uncertainties in the simulation.

In conclusion, our study underscores the potential of integrating information from the SI section to enhance the ability to detect pathological corneas. By considering corneal deformations along both meridians and introducing asymmetry-based indices, we offer a more comprehensive understanding of corneal behaviour in keratoconus. As the clinical analysis have revealed, the pathological area usually appears in the Temporal-Inferior quadrant of the eye, affecting more the SI plane with respect to the NT plane. This is the reason why the deformations of the SI plane are higher than the deformation of the NT during the NCT. Considering both the deformations, not only advances our knowledge of the disease but also holds promise for more accurate and early-stage pathology detection in clinical settings.

5. Conclusions and future works

The data obtained from the simulations highlight the potential improvements achievable by adjusting the Corvis ST operation. A 90-degree rotation of the camera during the clinical procedure can enhance the capability of the device to detect the presence of diseased tissue and its relative position when it is in the most typical position in the Nasal Inferior quadrant; while the asymmetry-based approach can be implemented through a more in-depth examination of the sectional images provided. The adding of the proposed adjustments in the clinical device can aid in the detection of keratoconus, even in the most challenging cases where no indications are discernible through topographic analysis. As a future endeavour, it could be beneficial to assess the indexes' capability to detect changes in material properties of the fellow eye of keratoconic patients, which may be at risk of developing the pathology. Furthermore, in a clinical context, it could be advantageous to perform multiple sectional analyses, considering the enhancement achieved in the numerical.

CRediT authorship contribution statement

Elena Redaelli: Writing – original draft, Methodology, Investigation, Formal analysis. **Michael Nana:** Methodology, Investigation. **Begoña Calvo:** Writing – review & editing, Supervision, Conceptualization. **José Félix Rodríguez Matas:** Writing – review & editing, Supervision. **Giulia Luraghi:** Writing – review & editing, Supervision. **Jos Rozema:** Writing – review & editing, Data curation. **Jorge Grasa:** Writing – review & editing, Supervision, Conceptualization.

Declaration of competing interest

The authors declare that they have no known competing financial interests or personal relationships that could have appeared to influence the work reported in this paper.

Fundings

This project has received funding from the European Union's Horizon 2020 research and innovation program under the Marie Skłodowska-Curie grant agreement No 956720 and the Department of Industry and Innovation (Government of Aragon), Spain through the research group Grant T24–20R (cofinanced with Feder 2014-2020: Construyendo Europa desde Aragon). Part of the work was performed by the ICTS "NANBIOSIS" specifically by the High Performance Computing Unit (U27), of the CIBER in Bioengineering, Biomaterials and Nanomedicne (CIBER-BBN at the University of Zaragoza).

Data availability

The data that has been used is confidential.

References

Ambekar, R., Toussaint, K.C., Wagoner Johnson, A., 2011. The effect of keratoconus on the structural, mechanical, and optical properties of the cornea. J. Mech. Behav. Biomed. Mater. 4 (3), 223–236.

Anderson, K., El-Sheikh, A., Newson, T., 2004. Application of structural analysis to the mechanical behaviour of the cornea. J. R. Soc. Interface 1 (1), 3–15.

Andreassen, T.T., Tjorth Simonsen, A., Oxlund, H., 1980. Biomeehanieal properties of keratoeonus and normal corneas. Exp. Eye Res. 31, 435–441.

Ariza-Gracia, M., Zurita, J., Piñero, D.P., Calvo, B., Rodríguez-Matas, J.F., 2016. Automatized patient-specific methodology for numerical determination of biomechanical corneal response. Ann. Biomed. Eng. 44 (5), 1753–1772.

Blackburn, B.J., Jenkins, M.W., Rollins, A.M., Dupps, W.J., 2019. A review of structural and biomechanical changes in the cornea in aging, disease, and photochemical crosslinking. Front. Bioeng. Biotechnol. 7 (MAR).

Curatolo, A., Birkenfeld, J.S., Martinez-Enriquez, E., Germann, J.A., Muralidharan, G., Palací, J., Pascual, D., Eliasy, A., Abass, A., Solarski, J., Karnowski, K., Wojtkowski, M., Elsheikh, A., Marcos, S., 2020. Multi-meridian corneal imaging of air-puff induced deformation for improved detection of biomechanical abnormalities. Biomed. Opt. Express 11 (11), 6337.

Daxer, A., Fratzl-fx, P., 1997. Collagen fibril orientation in the human corneal stroma and its implication in keratoconus. 38 (1), 121–129.

De Stefano, V.S., Dupps, W.J., 2017. Biomechanical diagnostics of the cornea. Int. Ophthalmol. Clin. 57 (3), 75–86.

Dev, L.-d., 2023. LS-DYNA Theory Manual.

Eliasy, A., Abass, A., Lopes, B.T., Vinciguerra, R., Zhang, H., Vinciguerra, P., Ambrósio, R., Roberts, C.J., Elsheikh, A., 2020. Characterization of cone size and centre in keratoconic corneas. J. R. Soc. Interface 17 (169).

Eliasy, A., Lopes, B.T., Wang, J., Abass, A., Vinciguerra, P., Bao, F.-j., Elsheikh, A., Eliasy, A., Lopes, B.T., Wang, J., Abass, A., Vinciguerra, P., Bao, F.-j., Introduction, A.E., 2023. Introduction and clinical validation of an updated biomechanically corrected intraocular pressure bIOP (v2) introduction and clinical validation of an updated biomechanically corrected. Curr. Eye Res. 48 (4), 382–391.

Ferrari, G., Rama, P., 2020. The keratoconus enigma: A review with emphasis on pathogenesis. Ocular Surface 18 (3), 363–373.

Gefen, A., Shalom, R., Elad, D., Mandel, Y., 2009. Biomechanical analysis of the keratoconic cornea. J. Mech. Behav. Biomed. Mater. 2 (3), 224–236.

Giraudet, C., Diaz, J., Le Tallec, P., Allain, J.M., 2022. Multiscale mechanical model based on patient-specific geometry: Application to early keratoconus development. J. Mech. Behav. Biomed. Mater. 129.

Guide, U., 2020. OCULUS Corvis® ST.

Hollingsworth, J.G., Bonshek, R.E., Efron, N., 2005. Correlation of the appearance of the keratoconic cornea in vivo by confocal microscopy and in vitro by light microscopy. Cornea 24 (4), 397–405.

Holzapfel, G.A., Gasser, T.C., Ogden, R.W., 2000. A new constitutive framework for arterial wall mechanics and a comparative study of material models. J. Elasticity 61 (1–3), 1–48.

Hr, P., 0000. OCULUS Pentacam® Pentacam® HR.

Li, X.F., Luo, S.L., Wang, Z., Miao, Y.Y., Zhu, M.M., Zheng, X.B., Luo, G.X., Bao, F.J., Chen, S.H., Wang, J.J., 2023. Dynamic topography analysis of the cornea and its application to the diagnosis of keratoconus. Comput. Biol. Med. 158 (March), 106800.

Lopes, B.T., Bao, F., Wang, J., Liu, X., Wang, L., Abass, A., Eliasy, A., Elsheikh, A., 2021. Review of in-vivo characterisation of corneal biomechanics. Med. Nov. Technol. Dev. 11 (March), 100073.

Meek, K.M., Blamires, T., Elliott, G.F., Gyi, T.J., Nave, C., 1987. Eye Diffraction Study Current Eye. Vol. 6. No. 7.

Meek, K.M., Boote, C., 2009. Progress in Retinal and Eye Research The use of X-ray scattering techniques to quantify the orientation and distribution of collagen in the corneal stroma. Progr. Retinal Eye Res. 28 (5), 369–392.

Meek, K.M., Tuft, S.J., Huang, Y., Gill, P.S., Hayes, S., Newton, R.H., Bron, A.J., 2005. Changes in collagen orientation and distribution in keratoconus corneas. Investigative ophthalmology & visual science 46 (6), 1948–1956.

Morishige, N., Wahlert, A.J., Kenney, M.C., Brown, D.J., Kawamoto, K., Chikama, T.-i., Nishida, T., Jester, J.V., 2007. Second-harmonic imaging microscopy of normal human and keratoconus cornea. Investigative ophthalmology & visual science 48 (3), 1087–1094.

Nash, I.S., Greene, P.R., Foster, C.S., 1982. Comparison of mechanical properties of keratoconus and normal corneas. Exp. Eye Res. 35 (5), 413–424.

Pandolfi, A., Manganiello, F., 2006. A model for the human cornea: Constitutive formulation and numerical analysis. Biomech. Model. Mechanobiol. 5 (4), 237–246.

Redaelli, E., Grasa, J., Calvo, B., Rodriguez Matas, J.F., Luraghi, G., 2022. A detailed methodology to model the Non Contact Tonometry: a Fluid Structure Interaction study. Front. Bioeng. Biotechnol. 10 (October), 1–12.

Roberts, C.J., Mahmoud, A.M., Bons, J.P., Hossain, A., Elsheikh, A., Vinciguerra, R., Vinciguerra, P., Ambrósio, R., 2017. Introduction of two novel stiffness parameters and interpretation of air puff-induced biomechanical deformation parameters with a dynamic Scheimpflug analyzer. J. Refract. Surg. 33 (4), 266–273.

Romero-Jiménez, M., Santodomingo-Rubido, J., Wolffsohn, J.S., 2010. Keratoconus: A review. Contact Lens Anterior Eye 33 (4), 157–166.

Roy, A.S., Dupps, W.J., 2011. Patient-specific computational modeling of keratoconus progression and differential responses to collagen cross-linking. Invest. Ophthalmol. Vis. Sci. 52 (12), 9174–9187.

Santodomingo-Rubido, J., Carracedo, G., Suzaki, A., Villa-Collar, C., Vincent, S.J., Wolffsohn, J.S., 2022. Keratoconus: An updated review. Contact Lens Anterior Eye 45 (3), 101559.

Tan, D.T., Dart, J.K., Holland, E.J., Kinoshita, S., 2012. Corneal transplantation. Lancet 379 (9827), 1749–1761.

Vellara, H.R., Patel, D.V., 2015. Biomechanical properties of the keratoconic cornea: A review. Clin. Exp. Optom. 98 (1), 31–38.

Vinciguerra, R., Ambrósio, R., Elsheikh, A., Roberts, C.J., Lopes, B., Morenghi, E., Azzolini, C., Vinciguerra, P., 2016. Detection of keratoconus with a new biomechanical index. J. Refract. Surg. 32 (12), 803–810.

Vinciguerra, R., Ambrósio, R., Roberts, C.J., Azzolini, C., Vinciguerra, P., 2017. Biomechanical characterization of subclinical keratoconus without topographic or tomographic abnormalities. J. Refract. Surg. 33 (6), 399–407.

Zhao, Y., Shen, Y., Yan, Z., Tian, M., Zhao, J., Zhou, X., 2019. Relationship among corneal stiffness, thickness, and biomechanical parameters measured by corvis st, pentacam and ora in keratoconus. Front. Physiol. 10 (JUN), 1–9.